Chaotic and multifractal characteristic analysis of noise of thermal variables from rotary kiln

Mingyang Lv · Xiaogang Zhang · Hua Chen · Yicong Zhou · Jianmin Li

Abstract In numbers of industrial fields, many filtering algorithms of industrial signals, mechanism-based modeling methods and control strategies are based on the hypothesis of white noise. However, some researchers propose that the colored noise is closer to the real noise than the white noise. Then, whether the noise is the white noise, the colored noise or other else? And what is the intrinsic dynamic characteristics of the noise? In this paper, noise signals of thermal variables from rotary kiln are extracted and their chaotic, statistical and multifractal characteristics are analyzed to answer the two questions. Based on the experimental results, it is the first time to discover that they are not the white noise or the monofractal colored noise but have the high-dimensional chaotic characteristic, that is, they are determinate and predictable for short term theoretically. However, some models are failed to predict them. Then, further experimental results imply those noise signals have both persistent and anti-persistent multifractal characteristics. In particular, the latter is a reason to failed predictions of noise signals. Moreover, it is firstly discovered that the multifractality of each noise signal is generated mainly by the long-term temporal correlation. Finally, two ideas about modeling multifractality of noise from rotary kiln are proposed as the future work.

Keywords Rotary kiln · Noise · Statistical characteristic analysis · Chaotic characteristic analysis · Multifractal characteristic analysis

M. Lv · X. Zhang (✉)
College of Electrical and Information Engineering, Hunan University, Changsha 410082, China
e-mail: zhangxg@hnu.edu.cn

H. Chen
College of Computer Science and Electronic Engineering, Hunan University, Changsha 410082, People's Republic of China

Y. Zhou
Department of Computer and Information Science, University of Macau, Macau, China

J. Li
College of Engineering and Design, Hunan Normal University, Changsha 410081, China

1 Introduction

The extensive presence of noise influences any system in real world. In particular, in industrial fields, noise interferes the detection of useful signals, like the detection of temperature signal and current signal. In order to conveniently characterize the noise in industrial fields, it is widely regarded as the white noise by many researchers. Then, many classical filtering algorithms, mechanism-based modeling methods and control strategies based on the hypothesis of white noise are proposed, for instance the Kalman filter and the subspace identification method. And, the robustness of many data-based techniques is evaluated by using the white noise. Furthermore, the hypothesis of white noise is widely used in other fields [1–4]. Nevertheless, the white noise is only a hypothesized ideal mathematical

model and does not really exist in real world. Some researchers in different fields pointed out that the colored noise-based hypothesis may be closer to the real noise than the white noise-based hypothesis [5–13]. For example, biological populations [10], geophysics [11], climate [12] and meteorological [13] are influenced by the environment variables with colored noise. Then, whether the noise from industrial fields is the white noise, the colored noise or other else?

There are many literatures about the noise. Some researchers proposed many algorithms to accurately generate known noise signals (the white noise, the pink noise and the brown noise) and studied their characteristics [14–17]. Some researchers analyzed behaviors of the noise from many practical dynamic systems and their influences to the practical dynamic systems (or models) in different fields [4,6,11–13,18–22]. Some researchers invented various methods to detect the useful signal from the environment with noise. Some researchers developed many denoising algorithms for the one-dimensional data [9,23] and the two-dimensional data [24–27]. Some researchers discussed noise reduction technologies in various actual fields, like aircraft noise reduction technologies [28]. Some researchers proposed many measurement methods of the noise in different fields, like the measurement method of the ultralow voltage noise in electronic devices [29]. Those works contribute the study and application of the noise in various fields. However, they do not involve the inherent dynamic characteristics (such as chaotic and multifractal behaviors) of the noise, except that the fractal behaviors of the monofractal noise (like the white noise and the colored noise) are analyzed. Moreover, some different kinds of time series (like the financial time series [30]) with random representations, mistakenly recorded as random before, have been discovered to exist intrinsic chaotic and multifractal characteristics, that is, the dynamic behaviors are the profounder view to recognize and distinguish the time series. Moreover, Gao [31] has discovered that the noise from dehydration tower of a chemical plant exists the high-dimensional chaotic characteristic. Enlightened by his discovery, the chaotic behavior of the noise from the rotary kiln is discovered. But the noise is not predictable for short term, which means the noise from the rotary kiln has other undiscovered behaviors. Thus, in this paper, based on previous studies about noise (especially Gao' work [31]), two questions are further explored: (1) What are the dynamic characteristics of noise from rotary kiln? (2) Whether the noise from rotary kiln is the white noise, the colored noise or other else?

The rotary kiln is a kind of large thermal equipment with many production links and widely used in metallurgy, building materials, steel and other fields. As the dynamic functions of the rotary kiln and its noise are unknown, in this paper, data-based methods are used to analyze the chaotic, statistical and multifractal characteristics of noise signals of thermal variables from rotary kiln. Firstly, those noise signals are extracted by using the frequency-based method and the time-based method, respectively. Secondly, the chaotic characteristics of noise signals are analyzed based on the phase space reconstruction (PSR) method [32,33] and the chaotic criterion. Then, the high-dimensional chaotic characteristic of those noise signals from the rotary kiln is discovered for the first time, which implies that those noise signals are determinate and theoretically predictable for short term. However, after further experiments, many models are failed to predict those determinate noise signals, which contradicts the short-term predictability of chaos. Thirdly, statistical characteristics of those noise signals are analyzed by the surrogate method [34–41]. And it is firstly discovered that the noise from the rotary kiln is not the white noise or the colored noise. Fourthly, in order to find out the reason of those failed predictions, multifractal characteristics of those noise signals are analyzed. Then, it is the first time to discover that each noise signal has both the persistent and anti-persistent multifractal characteristics. They are two contradictory features, which interactively together decide the whole correlation and fluctuation of the noise from rotary kiln. What is more, it also means the intrinsic dynamic mechanisms of noise from rotary kiln are more complex than those of the monofractal colored noise signals (like the pink noise and the brown noise). In particular, the anti-persistent multifractal characteristic is a reason why determinate noise signals from rotary kiln are predicted unsuccessfully, but it cannot negate the predictable characteristic of the noise from rotary kiln. Fifthly, based on contrast experiments, it is also firstly discovered that the multifractality of noise from rotary kiln is generated by the temporal correlation and wide probability density distribution together. In particular, the former is the main factor. Finally, based on the discoveries in our paper, previous works of multifractal theories and models [42–44], two ideas about modeling multifractality

of the noise signals are proposed as the future work in conclusion.

The rest sections of the paper are organized as follows: In Sect. 2, the study background and extraction of noise signals of thermal variables are introduced. In Sect. 3, chaotic characteristics of those noise signals are studied. In Sect. 4, the noise from the rotary kiln is distinguished from the white noise and the colored noise. In Sect. 5, multifractal characteristics of those noise signals are researched, the reason why some models are failed to predict those determinate noise signals is discovered, and the multifractal source of those noise signals is analyzed. In Sect. 6, the conclusion is summarized and two ideas about modeling multifractality of those noise signals are discussed.

2 Study background and extraction of noise of thermal variables

2.1 Study background

Parts of the rotary kiln equipment for sintering process are shown in Fig. 1a. And the schematic configuration of the sintering process of rotary kiln is shown in Fig. 1b, where the refractory steel cylinder whose length and diameter respective are 90–110 m and 3.5–4.5 m is installed obliquely with a small angle. Moreover, a sequence of physical changes and chemical reactions take place with the movement of the raw materials from the end of the kiln to the head of the kiln. Emphatically, the primary air mixed with the coal powders is spouted into the burning zone in which the raw materials are sintered into the clinkers. In particular, the rotary kiln contains five key thermal detection variables which are used to infer the sintering state of rotary kiln in practice, that is, the flame temperature (recorded as FT), the temperature of the head of the kiln (recorded as THK), the temperature of the end of the kiln (recorded as TEK), the current of the main motor (recorded as CMM) and the current of the cooling motor (recorded as CCM), where the FT is measured by the colorimetric pyrometer (recorded as CP), the THK and TTK are measured by the thermocouple, the CMM and the CCM are current of the motor which severally drive the refractory steel cylinder and cooler and they are measured by the current transformer. The measured general locations of the five key thermal detection variables are

labeled with red in Fig. 1a, b. And the measuring equipment is not drawn except the CP.

2.2 Extraction of noise signals of thermal variables

As the functions of the rotary kiln and its noise are both unknown, noise signals from rotary kiln will be analyzed by data-based methods in this paper. Then, it is a key to extract the noise signals from the above five thermal variables in this paper. However, it is a universal challenge to extract noise in many industrial fields. There are not universal denoising methods, and many researchers denoise based on limited information and their experience. Fortunately, there is an important criterion for extracting noise in many practical industrial processes (such as the rotary kiln), that is, compared with the slow change of effective signals, relative noise changes much fast along time [31,45]. Moreover, in order to ensure the analyzed results of noise signals of thermal variables from rotary kiln are credible and non-special, some works are carried out as follows:

(1) As the dynamic model of rotary kiln is unknown, all the thermal detection signals in this paper are not simulate data but real data which are collected from the Inner Mongolia branch of China Datang Corporation.

(2) Two groups of real thermal detection signals with different sintering conditions are chosen and recorded as G1 and G2 where each group contains above five key thermal detection signals, as shown in Fig. 2. What is more, each series contains 10,000 sampling points and each sampling interval is 1 min, that is, the time length of each series is about 7 days, which can reflect most of the sintering conditions of rotary kiln.

(3) The methods based on the frequency and based on the time are, respectively, used to extract noise from above two groups of thermal detection signals (G1 and G2). One is the wavelet package decompose (WPD) method [46,47]. It is the frequency-based method and introduced in "Appendix A.1." Then, the extracted noise signals from G1 and G2 are, respectively, recorded as G1_wpd (including wpd1, wpd2, wpd3, wpd4 and wpd5) and G2_wpd (including wpd6, wpd7, wpd8, wpd9 and wpd10), as shown in Figs. 3 and 4. The other method is called the Gao method and introduced in "Appendix A.2" in this paper. Its

(a)
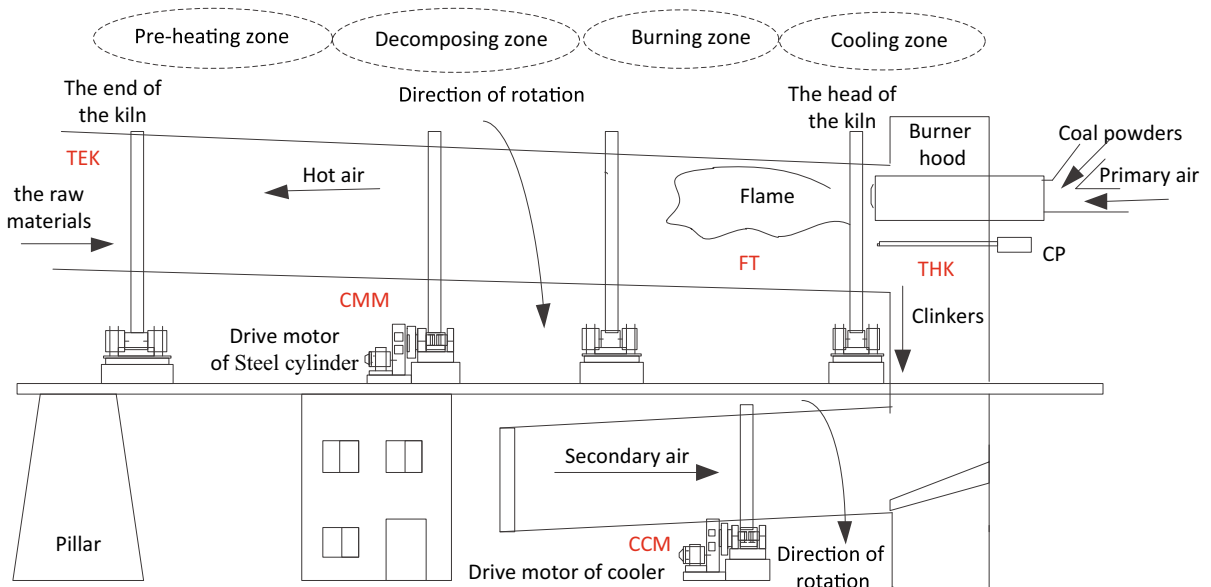
(b)

Fig. 1 **a** Parts of the rotary kiln equipment for sintering process in the Inner Mongolia branch of China Datang Corporation. **b** The schematic configuration of the sintering process of rotary kiln

nature is the moving average, and it is the time-based method. The extracted noise signals from G1 and G2 are, respectively, recorded as G1_Gao (including Gao1, Gao2, Gao3, Gao4 and Gao5) and G2_Gao (including Gao6, Gao7, Gao8, Gao9 and Gao10), as shown in Figs. 3 and 4.
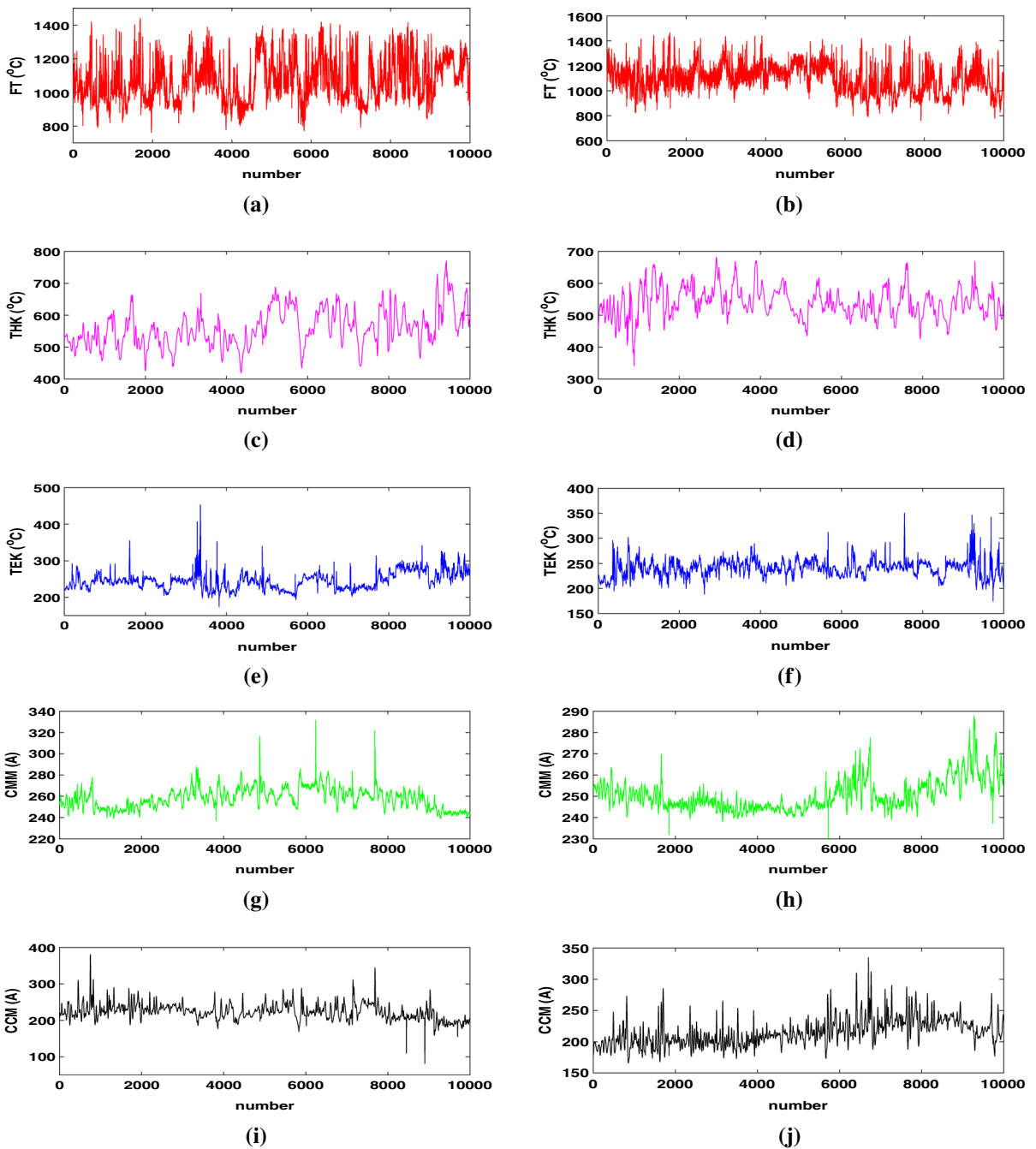
Fig. 2 Two groups of original data (G1 and G2). The G1 contains (**a**, **c**, **e**, **j**, **i**), and the G2 contains (**b**, **d**, **f**, **h**, **j**). And the same thermal detection variables are drawn with same color. (Color figure online)

Those extracted noise signals are from different parts of rotary kiln, and their original thermal signals do not belong to the same type of signal. Thus, if all the noise signals have some same characteristics, then the same characteristics are believable. Moreover, contrasted with the original thermal signals in Fig. 2, the extracted noise signals in Figs. 3 and 4 seem more disorder, which may indicate that the noise signals are
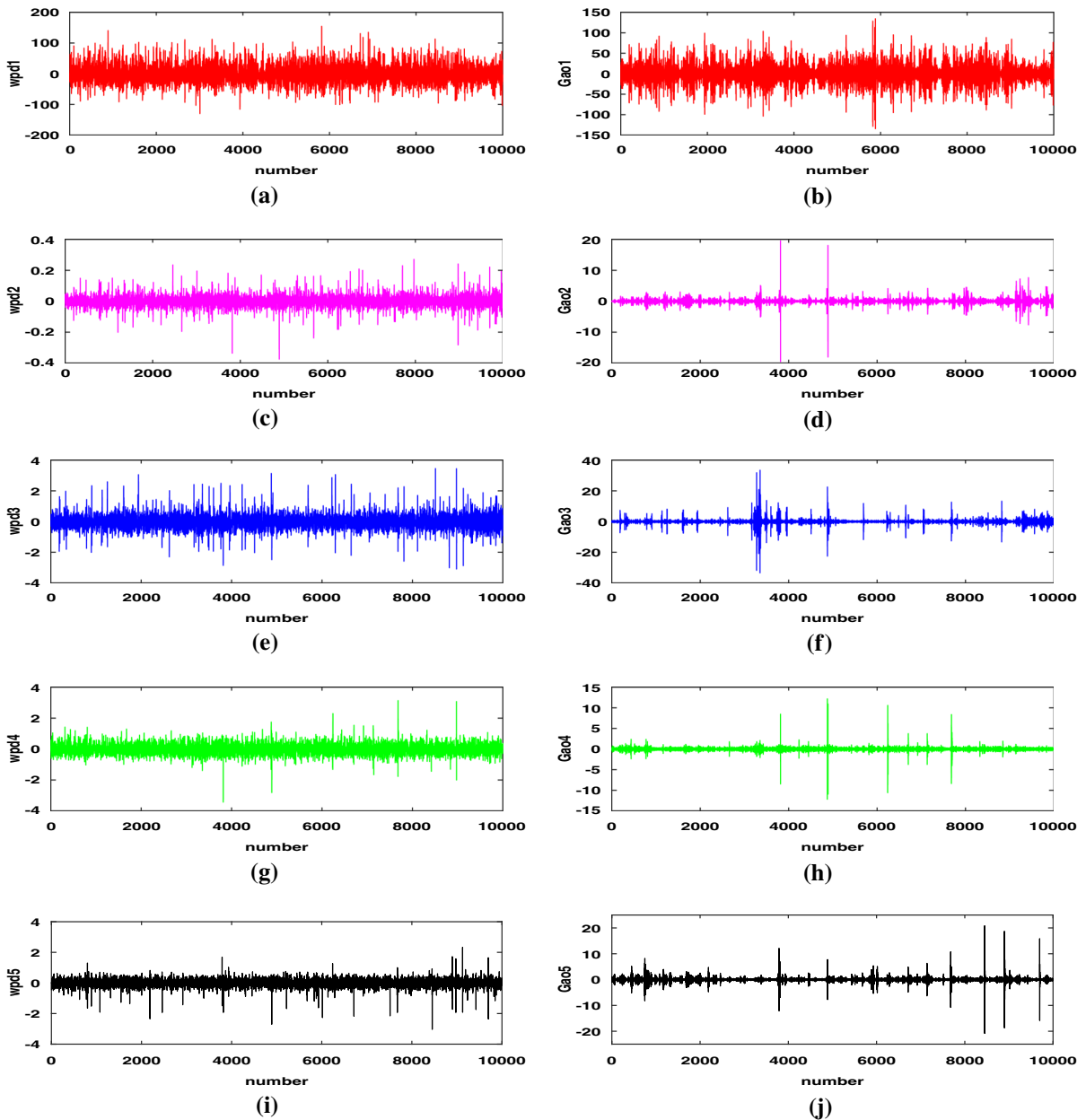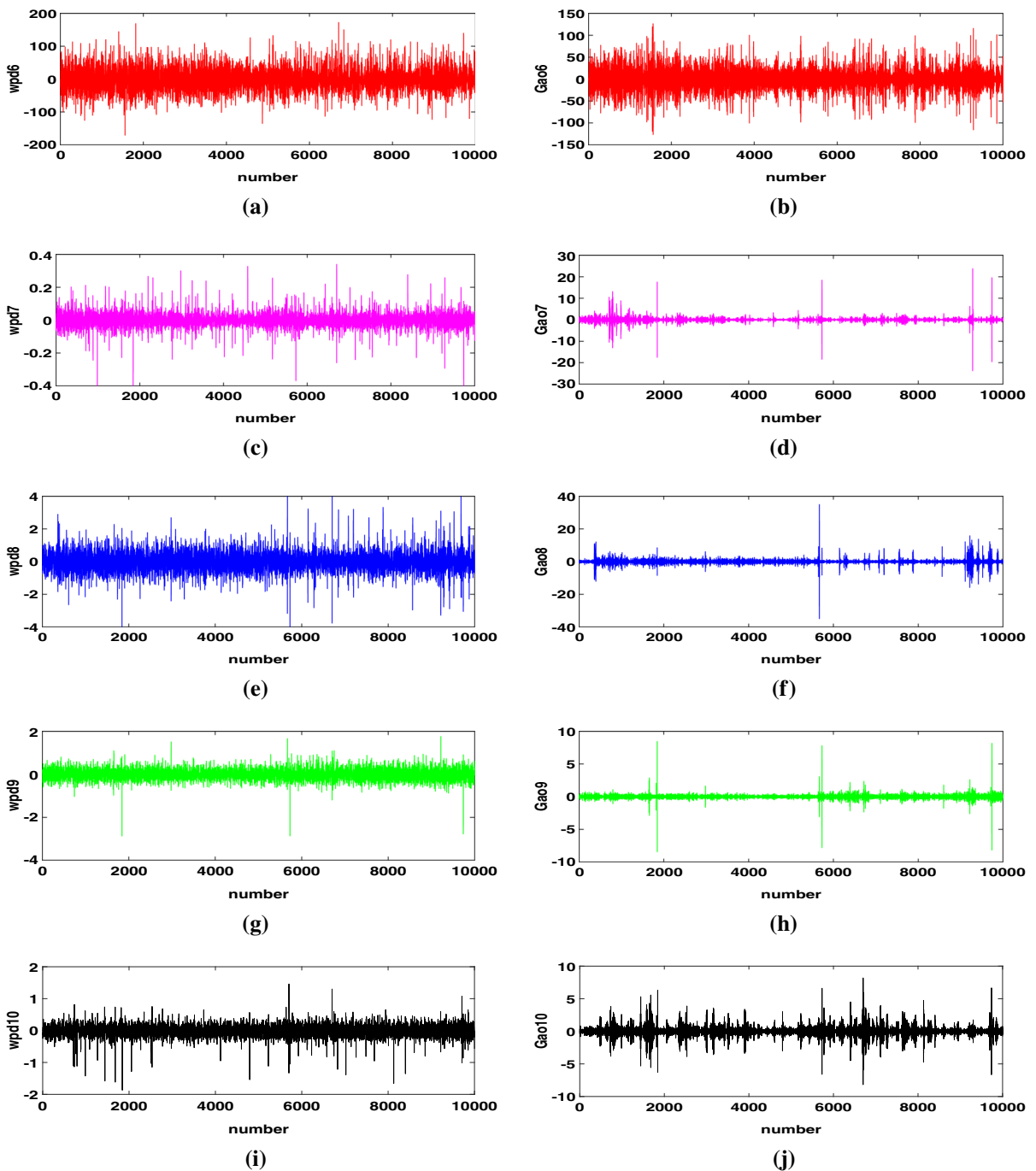
Fig. 3 Two groups of noise signals from the G1. G1_wpd means five noise signals are extracted from G1 by the WPD method and, respectively, displayed in (**a**, **c**, **e**, **j**, **i**). G1_Gao means five noise signals are extracted from G1 by the Gao method and, respec- tively, displayed in (**b**, **d**, **f**, **h**, **j**). And noise signals from same thermal detection variable are drawn with same color. (Color figure online)

random without any deterministic mechanism. In particular, for distinguishing five kinds of signals conveniently, the same thermal detection signals and relative noise signals are drawn with the same color in this paper.

3 Chaotic characteristic analysis

If dynamical function is known, chaotic analysis can be executed like the reference [48,49]. However, the dynamical functions of the rotary kiln and its noise are

Fig. 4 Two groups of noise signals from the G2. G2_wpd means five noise signals are extracted from G2 by the WPD method and, respectively, displayed in (**a**, **c**, **e**, **j**, **i**) and G2_Gao means five noise signals are extracted from G1 by the Gao method and, respectively, displayed in (**b**, **d**, **f**, **h**, **j**). And noise signals from same thermal detection variable are drawn with same color. (Color figure online)

unknown, the chaotic analysis of noise signals from rotary kiln is accomplished based on the PSR method

[32,33] and some chaotic criteria; for example, the fractal dimension must be finite and non-integer, one of the

Lyapunov exponents must be positive at least, and the Kolmogorov entropy must be finite and positive. If one of the above three criteria is satisfied, those noise signals are chaotic.

3.1 Phase space reconstruction method

Based on the PSR method [32,33], the one-dimensional noise $\{x_i \mid i = 1, \ldots, N\}$ can be expanded into an m-dimension phase space to achieve its inner dynamic characteristics as follows:

$$\mathbf{Y}_j = (x_j, x_{j+t}, \ldots, x_{j+(m-1)t}), \tag{1}$$

where $\mathbf{Y}_j \, (j = 1, \ldots, M)$ is the m-dimension state vector and represents the state of system at any time. M is the number of reconstructed phase points and satisfies $M = N - (m - 1)t$, and m is the embedding dimension. t is the index lag, if the sampling interval is τ_s, then the delay time $\tau = t\tau_s$, so t and τ_s are not distinguished unless necessary. Moreover, the PSR method contains two parameters: one is the delay time which is estimated by the mutual information (MI) method [50]; another is the embedding dimension which is estimated by the false nearest neighbor (FNN) method [51] in this paper.

The mutual information of the series x_i (recorded as X) and its delay time series x_{i+t} (recorded as $X + t$) are defined as follows:

$$I(X, X + t) = H(X) + H(X + t) - H(X, X + t), \tag{2}$$

where $I(X, X + t)$ is the mutual information of the series X and $X + t$, $H(X)$ and $H(X + t)$ represent the entropy of the series X and $X + t$, respectively, $H(X, X + t)$ is the joint entropy of the series X and $X + t$. For each t, there is a mutual information value, that is, the mutual information is the function of t. And the optimal delay time is relative to the first minimum of the function. As shown in Figs. 5 and 6, each optimal delay time point of the noise signals is highlighted. Moreover, when $t = 0$, the mutual information of X and X is the biggest. Then, in order to display the optimal delay time point visibly, the point with $t = 0$ is not drawn in Figs. 5 and 6. Please see reference [50] for the details.

After the one-dimensional time series is embedded into m-dimensional Euclidean space, the distance between any phase point $\mathbf{Y}_j$ and its nearest phase point $\mathbf{Y}_i$ is:

$$R_m(j) = \left\| \mathbf{Y}_j - \mathbf{Y}_i \right\|_2 = \left[\sum_{k=0}^{m-1} (x_{j+kt} - x_{i+kt}) \right]^{\frac{1}{2}}, \tag{3}$$

where the definition of the phase points $\mathbf{Y}_j$ and $\mathbf{Y}_i$ is in Eq. (3) and $\|\cdot\|_2$ represents the 2-norm in the Euclidean space. Then, when the one-dimensional time series is embedded into $(m + 1)$-dimension Euclidean space, the new distance between them is:

$$\begin{aligned} R_{m+1}(j) &= \left\| \mathbf{Y}_j - \mathbf{Y}_i \right\|_2 \\ &= \left[\sum_{k=0}^{m-1} (x_{j+kt} - x_{i+kt}) \right]^{\frac{1}{2}} \\ &= \left[R_d^2(j) + (x_{j+mt} - x_{i+mt})^2 \right]^{\frac{1}{2}}; \end{aligned} \tag{4}$$

then,

$$\left[\frac{R_{d+1}^2(j) - R_d^2(j)}{R_d^2(j)} \right]^{\frac{1}{2}} = \frac{|x_{j+mt} - x_{i+mt}|}{R_d(j)}, \tag{5}$$

making

$$R_j = \frac{|x_{j+mt} - x_{i+mt}|}{R_d(j)}. \tag{6}$$

$\mathbf{Y}_i$ will be a false nearest neighbor of the phase points $\mathbf{Y}_j$ when R_j is bigger than R_{tol}, a given threshold. For each m, the number of false nearest neighbors points of all the phase points is counted to calculate the percentage of the false nearest neighbor points (recorded as FNN percentage), that is, the FNN percentage is the function of m. In theory, the optimal embedding dimension m is relative to the FNN percentage which drops to 0%, but in practice, it is small enough when the FNN percentage drops to 1%. The result is drawn in Fig. 7.

3.2 Estimation of largest Lyapunov exponent

Chaotic system is extremely sensitive to the initial conditions, that is, two initially close trajectories will diverge along with time, and the diverging behavior is measured quantitatively by the Lyapunov exponent [52]:

$$d(t) = e^{\lambda t}, \tag{7}$$
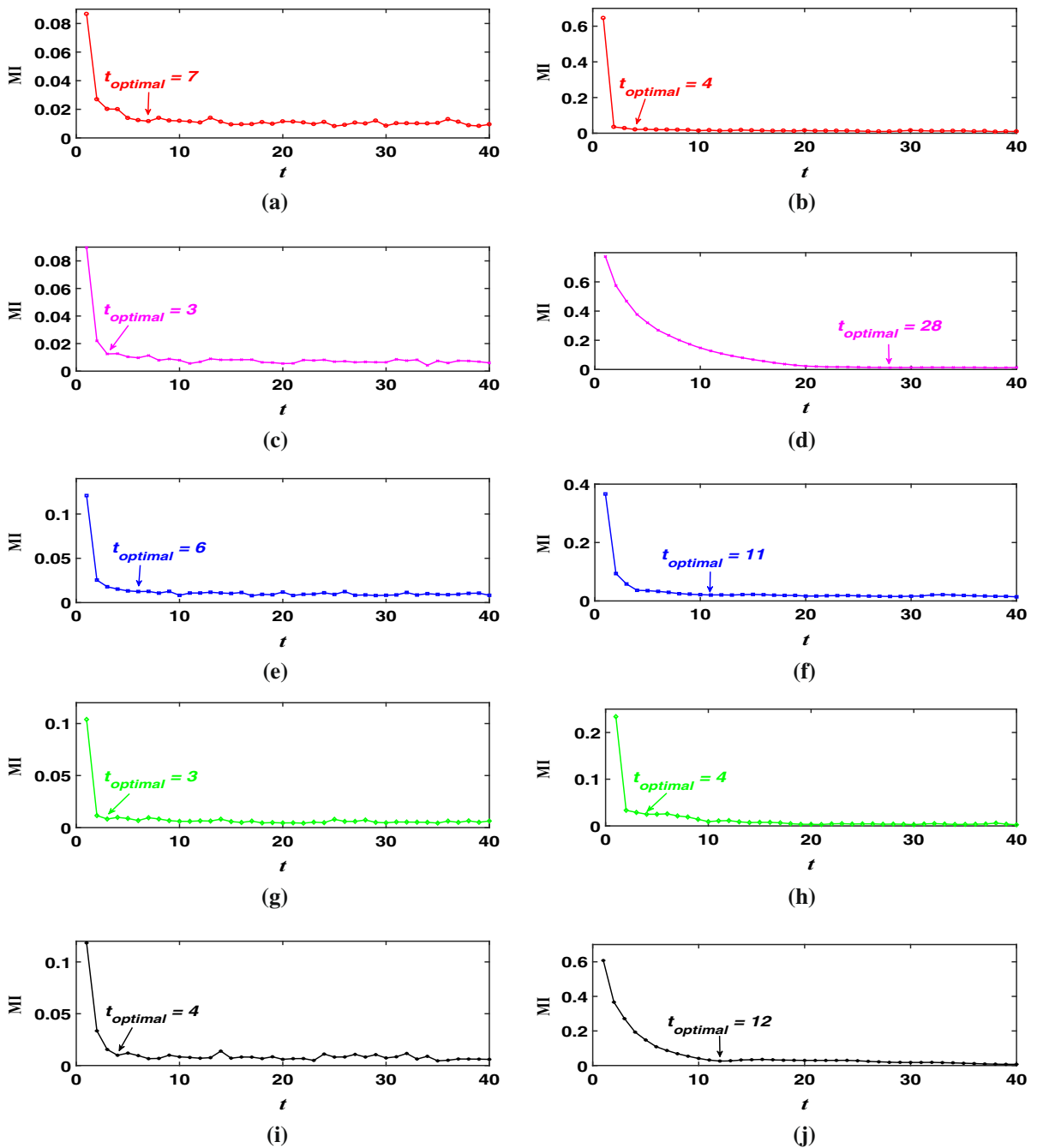
Fig. 5 Mutual information (MI) curves of the G1. **a** wpd1, **b** gao1, **c** wpd2, **d** gao2, **e** wpd3, **f** gao3, **g** wpd4, **h** gao4, **i** wpd5, **j** gao5. And noise signals from same thermal detection variable are drawn with same color. (Color figure online)

where $d(t)$ stands for the diverging distance between two phase points at time t and λ is the Lyapunov exponent. Wolf [52] proposed the method to estimate the Lyapunov exponent spectrum in which the Lyapunov

exponents are arranged from large to small. As the Lyapunov exponent represents divergence of dynamic system, the sum of Lyapunov exponents of dissipative system must be negative [53], that is, if the dynamic system
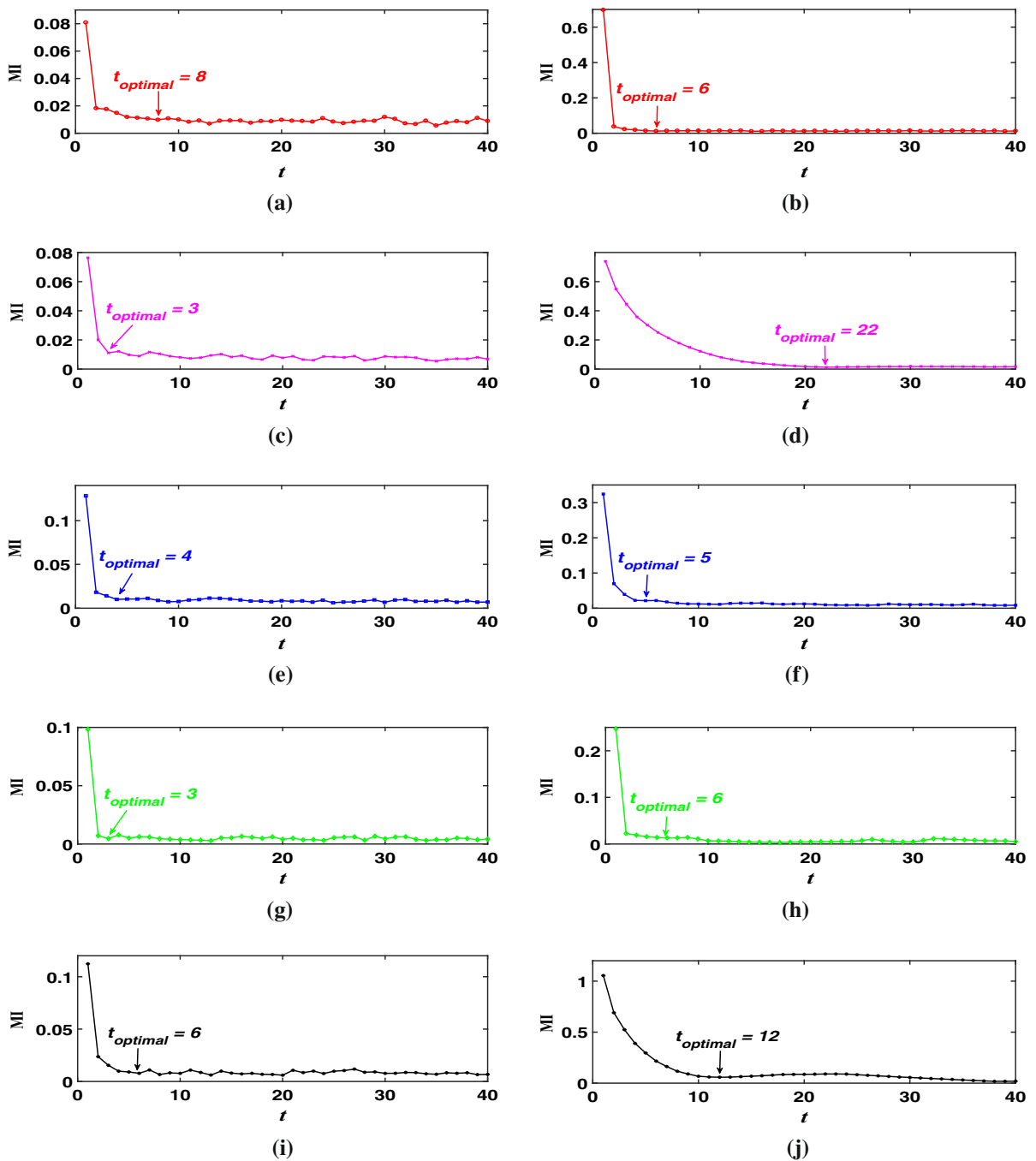
Fig. 6 Mutual information (MI) curves of the G2. **a** wpd6, **b** gao6, **c** wpd7, **d** gao7, **e** wpd8, **f** gao8, **g** wpd9, **h** gao9, **i** wpd10, **j** gao10. And noise signals from same thermal detection variable are drawn with same color. (Color figure online)

is chaotic, its largest Lyapunov exponent must be positive. Then, the largest Lyapunov exponent (recorded as λ_1) is estimated by the Wolf method which is simply introduced as follows. Set $Y(t_0)$ is a phase point in

reconstructed phase space, and its nearest phase point is $Y_0(t_0)$; then, the distance between them is L_0. The distance of the two points increases along with time. If the distance is bigger than the given value ε at time t_1, that

(a)

(b)

(c)

(d)
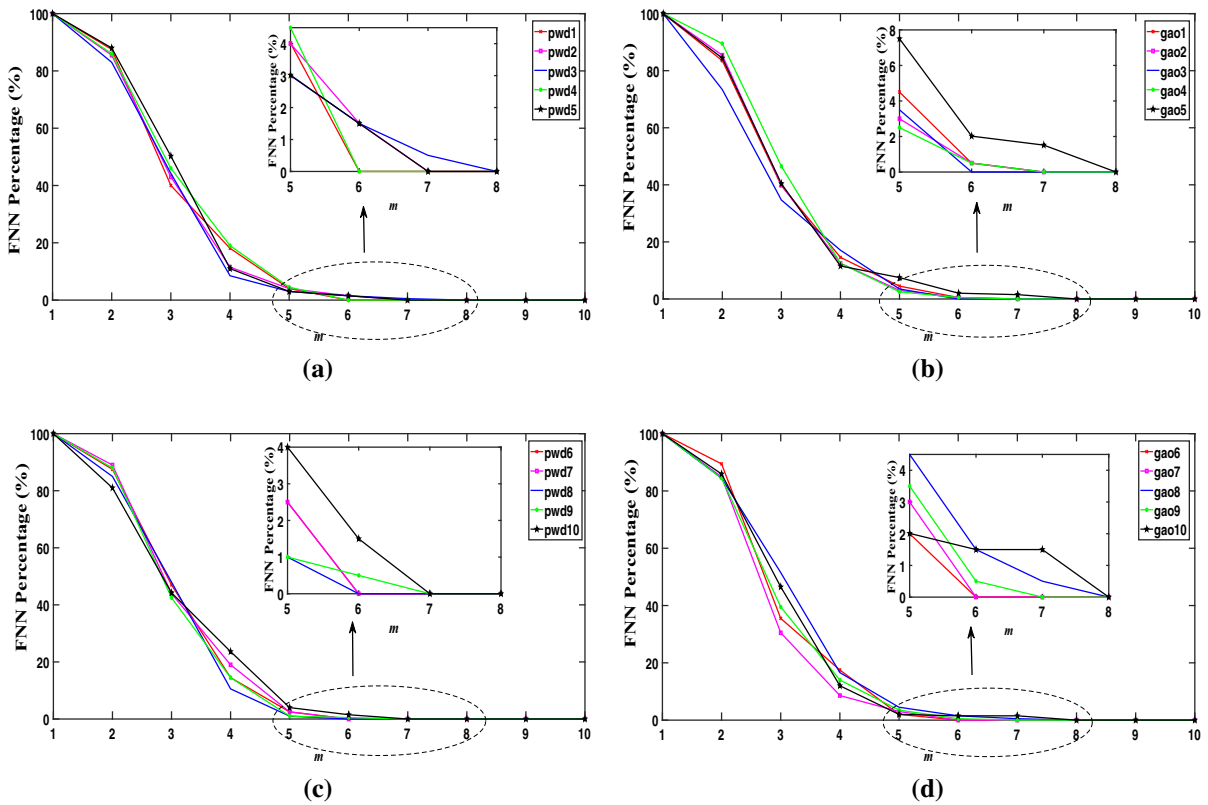
Fig. 7 False nearest neighbor (FNN) curves. **a** G1_wpd, **b** G1_gao, **c** G2_wpd, **d** G2_gao. And noise signals from same thermal detection variable are drawn with same color

is, $L_0' = |Y(t_1) - Y_0(t_1)| > \varepsilon$, the two trajectories are diverged. Then, a fit point $Y_1(t_1)$ should be sought out in the neighborhood of $Y(t_1)$, and the point $Y_1(t_1)$ must satisfy two conditions: 1) $L_1 = |Y(t_1) - Y_1(t_1)| < \varepsilon$; 2) $Y(t_1)$ and $Y_1(t_1)$ construct a line, and $Y(t_1)$ and $Y_0(t_1)$ also construct a line; then, the angle between the two lines must be the smallest. Then, the above process is repeated n times, as shown in Fig. 8. And the largest Lyapunov exponent is estimated by averaging the diverging distance of the n iterations:

$$\lambda_1 = \frac{1}{t_n - t_0} \sum_{i=0}^{n-1} \ln \frac{L_i'}{L_i} = \frac{1}{n} \sum_{i=0}^{n-1} \ln \frac{L_i'}{L_i}. \tag{8}$$

3.3 Results and analysis

Results of the chaotic characteristic analysis are shown in Table 1. Despite that all the largest Lyapunov expo-
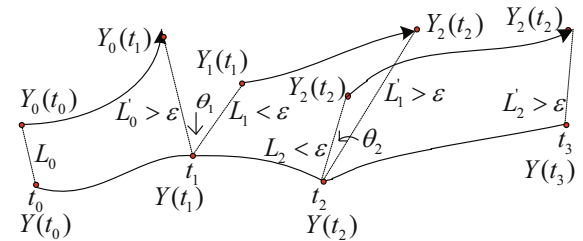
Fig. 8 Schematic configuration of the Wolf method

nents are not the same, it is obvious that they are all positive, which is a strong indication to the presence of the chaotic characteristic in noise signals from rotary kiln, that is, the noise from rotary kiln is determinate signal rather than random or the white noise. Moreover, as all $m > 3$, the noise from rotary kiln is high-dimensional chaotic which implies the dynamics of the noise from rotary kiln is very complex. Besides, Gao [31] also discovered that the noise signal from dehydration tower of a chemical plant has the high-dimensional chaotic.

Table 1 Chaotic characteristics of noise from rotary kiln (where the t is the delay time, the m is the embedding dimension and the λ_1 is the largest Lyapunov exponent)

	t	m	λ_1		t	m	λ_1
wpd1	7	5	0.5490	Gao1	4	6	0.1770
wpd2	3	6	0.1470	Gao2	28	6	0.0547
wpd3	6	7	0.1510	Gao3	11	5	0.1666
wpd4	3	5	0.3477	Gao4	4	6	0.0836
wpd5	4	6	0.1746	Gao5	12	7	0.0263
wpd6	8	5	0.4123	Gao6	6	5	0.3091
wpd7	3	5	0.2123	Gao7	22	5	0.0682
wpd8	4	5	0.3250	Gao8	5	7	0.0903
wpd9	3	6	0.3194	Gao9	6	6	0.1811
wpd10	6	6	0.4167	Gao10	12	7	0.0617

Thus, the two discoveries imply noise from many industrial fields may have the chaotic characteristic.

Theoretically, the chaos is predictable for short term [53], that is, the noise from rotary kiln is predictable. Then, several models are used to predict the noise signals from rotary kiln but failed. Maybe, the noise from rotary kiln has some undiscovered characteristics which impede effective prediction of noise.

4 Statistical characteristic analysis based on the surrogate method

The surrogate data method introduced by Theiler [34] is used to detect the characteristic of data. The method contains two steps: The first step is to generate the surrogate data through reserving certain properties of original data and destroying others, and generated surrogates are corresponding to a designated null hypothesis. The second step is to choose discriminative statistics to measure the original data and each surrogate. If the discriminative statistic exists a significant difference, the null hypothesis is rejected, that is, the original data and the surrogates are not from the same dynamic process, vice versa. There are many surrogate methods for different kinds of data [34–41]. Among of them, two linear surrogate methods proposed by Theiler [34] are discussed here to distinguish the noise from the white noise and the colored noise. One is that the data are from the independent identically distributed (IID) random process and related surrogate data are generated by the random shuffle (RS) algorithm. The other is that the data are from a linearly filtered IID noise process and related surrogate data are generated by the Fourier transform (FT) algorithm. Other researchers

further pointed out that the former and the latter are, respectively, regarded as the null hypotheses of the white noise and colored noise [36,54,55]. Thus, if the two null hypotheses are rejected, the noise can be distinguished from the white noise and the colored noise.

4.1 The surrogate analysis based on the null hypotheses of the white noise

Small [36] pointed out that the surrogate data generated by the RS algorithm have the same probability distribution as the original data, but have not temporal correlation, that is, if the noise from the rotary kiln has temporal correlation, they are not the white noise. Therefore, the surrogate analysis process could be simplified, that is, the temporal correlation of only the noise from the rotary kiln need be checked by the Ljung–Box Q-test (LBQ test) which is defined as follows:

$$Q = N(N+2) \sum_{k=1}^{l} \frac{\hat{\rho}_k^2}{N-h}, \tag{9}$$

where N is the number of the series, l is the sum of autocorrelation lags, and ρ_k is the autocorrelation at lag k and $\hat{\rho}_k$ is the estimated value of ρ_k. And the null hypothesis is that the first l autocorrelations are jointly zero, that is, $H0 : \rho_1 = \rho_2 = \cdots = \rho_l = 0$. Under the null hypothesis, the asymptotic distribution of Q is Chi-square with l degrees of freedom.

The results are shown in Table 2. And it is obvious that each noise from the rotary kiln has temporal correlation, that is, the noise from the rotary kiln is not the white noise.

Table 2 Results of LBQ test of the noise from the rotary kiln

	p value of LBQ test		p value of LBQ test
wpd1	0	Gao1	0
wpd2	0	Gao2	0
wpd3	0	Gao3	0
wpd4	0	Gao4	0
wpd5	0	Gao5	0
wpd6	0	Gao6	0
wpd7	0	Gao7	0
wpd8	0	Gao8	0
wpd9	0	Gao9	0
wpd10	0	Gao10	0

4.2 The surrogate analysis based on the null hypotheses of the colored noise

The null hypothesis is that the noise from the rotary kiln is colored noise. Moreover, the related surrogate data are generated by the Fourier transform algorithm (please see [34] for the detail). The number of the surrogate data is chosen based on the conclusion of the Theiler [34], that is, for a two-sided test, $M = 2K/\alpha - 1$ surrogates should be generated, where K is a positive integer and α is the probability of false rejection corresponding to a level of significance $(1 - \alpha) \times 100\%$. As larger values of K will make a more sensitive test than $K = 1$, $K = 1$ is used here to minimize the computational effort of generating surrogates [37]. Then, 39 surrogate data should be generated at least for two-sided tests at a significance level of 95%. Moreover, the more surrogates are used; the more believable the test is [37], then 128 surrogates are generated here for each of the noise data. There are many discriminating statistics for the test, such as the prediction error, correlation dimension, entropy and the largest Lyapunov exponent. As the calculations of the correlation dimension and the entropy involve the selection of linear range, the results are influenced easily. In particular, some monofractal colored noise also have the correlation dimension. Moreover, as the noise from the rotary kiln cannot be availably predicted, the prediction error also cannot be used as the discriminating statistic. Then, the largest Lyapunov exponent is used as the discriminating statistic, which can be regarded as a further detection. And the significance S of the discriminating statistic is computed as follows:

$$S = \frac{|\lambda_1 - \overline{\lambda}|}{\sigma_\lambda}, \tag{10}$$

where the λ_1 is the largest Lyapunov exponent of the original noise; the $\overline{\lambda}$ and the σ_λ, respectively, are the mean and standard deviation of the related surrogate data. Under the assumption of Gaussian distribution of statistic largest Lyapunov exponent (λ), the value of $S > 1.96$ indicates that the null hypothesis will be rejected at 0.05 significance level, that is, the original noise is not random but deterministic. What is more, the p value of the S is a probability of observing a significance S. When $p < 5\%$, the null hypothesis is rejected. Moreover, the p value is given by the Gaussian error function, that is, $p = \mathrm{erfc}(S/\sqrt{2})$. And the Gaussian error function erfc is calculated as follows:

$$\mathrm{erfc}(x) = 1 - \frac{2}{\sqrt{\pi}} \int_x^\infty e^{-t^2} \mathrm{d}t. \tag{11}$$

The results of the surrogate analysis are displayed in Tables 3 and 4. It is obvious that all the values of the significance S are bigger than 1.96 both in Tables 3 and 4. And all the values of the p value are less than 5% both in Tables 3 and 4. Thus, the null hypothesis should be rejected and the noise from the rotary kiln is not colored noise.

Thus, based on above surrogate analyses, we confirm that the noise from the rotary kiln is neither the white noise nor the colored noise.

5 Multifractal characteristic analysis

Based on above experimental results, the noise signals from rotary kiln are not the white noise but determinate signals with correlation. As the colored noise signal is also correlative, whether the noise signals from rotary kiln are the colored noise signals? Moreover, because the colored signals are monofractal in nature, the multifractal trend fluctuation analysis (MFDFA) method [56] is used to analyze the multifractal characteristics of the noise signals from rotary kiln to distinguish them from the monofractal colored noise.

5.1 Overview of MFDFA method and multifractal characteristics

Assume that there is a time series x_i with length N, then the MFDFA method is summarized as follows [56].

Table 3 Results of the surrogate analysis of the G1

	wp1	wp2	wp3	wp4	wp5	Gao1	Gao2	Gao3	Gao4	Gao5
λ_1	0.5490	0.1470	0.1510	0.3477	0.1746	0.1770	0.0547	0.1666	0.0836	0.0263
$\overline{\lambda}$	0.7777	0.6262	0.5782	0.6965	0.6443	0.5912	0.2392	0.6329	0.4510	0.2407
σ_λ	0.0886	0.0949	0.0634	0.0964	0.0892	0.0819	0.0425	0.0742	0.0742	0.0455
S	2.5809	5.0479	6.7383	3.6194	5.2670	5.0587	4.3421	6.2840	4.9511	4.7114
p	0.0099	4.47E−07	1.60E−11	0.0003	1.39E−07	4.22E−07	1.41E−05	3.30E−10	7.38E−07	2.46E−06

The λ_1 is the largest Lyapunov exponent of the original noise, the $\overline{\lambda}$ and the σ_λ, respectively, are the mean and standard deviation of the related surrogate data, S is the significance, and p is the p value

Table 4 Results of the surrogate analysis of the G2

	wp6	wp7	wp8	wp9	wp10	Gao6	Gao7	Gao8	Gao9	Gao10
λ_1	0.4123	0.2123	0.3250	0.3194	0.4167	0.3091	0.0682	0.0903	0.1811	0.0617
$\overline{\lambda}$	0.7910	0.8005	0.7355	0.5805	0.6692	0.7677	0.3534	0.4692	0.5442	0.1320
σ_λ	0.0818	0.0914	0.0924	0.0939	0.0774	0.0813	0.0528	0.0576	0.0771	0.0292
S	4.6281	6.4375	4.4415	2.7816	3.2626	5.6382	5.3984	6.5824	4.7108	2.4056
p	3.69E−06	1.21E−10	8.93E−06	0.0054	1.10E−03	1.72E−08	6.72E−08	4.63E−11	2.47E−06	1.61E−02

The λ_1 is the largest Lyapunov exponent of the original noise, the $\overline{\lambda}$ and the σ_λ, respectively, are the mean and standard deviation of the related surrogate data, the S is the significance, and the p is the p value

(1) The cumulative deviation sequence $Y(i)$ of the time series x_i is calculated by

$$Y(i) = \sum_{k=1}^{i}(x_k - \bar{x}), i = 1, \ldots, N, \qquad (12)$$

where $\bar{x}$ is the mean of the time series x_i.

(2) The series $Y(i)$ is divided into N_s non-overlapping segments and the length of each segment is s, that is, $N_s = [N/s]$, where $[\cdot]$ means that the number is rounded down to the nearest integer. Then, the local variance of each segment $v(v = 1, \ldots, N_s)$ is calculated by

$$F^2(v, s) = \frac{1}{s} \cdot \sum_{i=1}^{s} \{Y[(v - 1)s + i] - y_v(i)\}^2, \qquad (13)$$

where $y_v(i)$ is the local trend function in segment v and fitted by the m order polynomial based on the least square method. Considering that big value of m will lead to over fitting, m is set 1 in this paper, as the values of the N_s are not all integers, that is, a short section of data whose length less than s at end of the series remains. To use the whole data, the same computational procedure is repeated from

the end to the head. Thus, $2N_s$ intervals with the same length are obtained. Then, the local variance of each segment $v(v = N_s + 1, \ldots, 2N_s)$ is calculated by

$$F^2(v, s) = \frac{1}{s} \sum_{i=1}^{s} \{Y[N - (v - N_s)s + i] - y_v(i)\}^2, \qquad (14)$$

(3) By averaging the local variances in all segments, the qth-order fluctuation function for each scale s is obtained as

$$F_q(s) = \left\{ \frac{1}{2N_s} \sum_{v=1}^{2N_s} [F^2(v, s)]^{q/2} \right\}^{1/q}, \quad q \neq 0, \qquad (15)$$

$$F_0(s) = \exp \left\{ \frac{1}{4N_s} \sum_{v=1}^{2N_s} \ln[F^2(v, s)] \right\}, \quad q = 0. \qquad (16)$$

(4) Based on Eq. (17), the slope of double logarithmic plot of $F_q(s)$ versus s for each q is estimated by the least square fit, and the slope is called as the gener-

alized Hurst exponent or qth-order Hurst exponent $h(q)$:

$$F_q(s) \sim s^{h(q)}. \tag{17}$$

Theoretically, $h(q)$ is a function of q for multifractal series and a constant independent of q for monofractal series. Meanwhile, qth-order scaling exponent $\tau(q)$, also called mass exponent, is expressed as

$$\tau(q) = qh(q) - 1. \tag{18}$$

As $h(q)$ is a constant independent of q for the monofractal series, it is obvious that $\tau(q)$ is linear with q for monofractal series. However, $\tau(q)$ is nonlinear with q for multifractal series.

Through the Legendre transformation [57,58], another quantitative measurement of the multifractal characteristic is the singularity spectrum or multifractal spectrum $f(\alpha)$:

$$\alpha = \tau'(q), \tag{19}$$
$$f(\alpha) = \alpha q - \tau(q) \tag{20}$$

where α is called the Holder exponent or the singularity exponent and $f(\alpha)$ is the singularity dimension of sub-series with the same Holder exponent α. And the two parameters (α and $f(\alpha)$) constitute the multifractal spectrum. Moreover, for the monofractal, $\alpha = \tau'(q) = h(q)$ is based on Eqs. (18) and (19); then, $f(\alpha) = 1$ in Eq. (20). Meanwhile, $h(q)$ is constant (recorded as c) and $h'(q) = 0$, $\alpha = \tau'(q) = h(q) + qh'(q) = c$ is based on Eqs. (18) and (19), that is, theoretically, for the monofractal, the values of the Holder exponent α and the Hurst exponent $h(q)$ are equal, and there is only one point $(c, 1)$ in the multifractal spectrum.

In order to intuitively show the differences between the colored noise and the noise from rotary kiln, the qth-order Hurst exponent, the qth-order scaling exponent and the multifractal spectrum are used to measure their multifractal characteristics. Please see reference [30, 56,59] about the detail of the multifractal theory.

5.2 Multifractal analysis of two kinds of monofractal colored noise

The power-law noise is a general term for a class of noise, like the white noise, the pink noise and the brown noise. And they have been seen and studied as the background noise in many fields [11–13]. Moreover, they have some statistical features. Like, there is a power relationship between their power spectral densities and the frequency as follows:

$$S(f) \propto 1/f^{\alpha}, \tag{21}$$

where the $S(f)$ is the power spectral density and the f is the frequency. In particular, the α is real valued and $\alpha \in [-2, 2]$. This is the reason why they are called as the power-law noise. For the white noise, $\alpha = 0$, that is, $S(f)_{White} \propto 1/f^0$. For the pink noise, $\alpha = 1$, that is, $S(f)_{Pink} \propto 1/f$. For the brown noise, $\alpha = 2$, that is, $S(f)_{Brown} \propto 1/f^2$. In this paper, two kinds of monofractal colored noise (pink noise and brown noise) taken as an example are compared to the noise from the rotary kiln. The two kinds of noise are generated using the following commends based on DSP System Toolbox in MATLAB 2016b.

whiteNoise = dsp.ColoredNoise(0,1e4,1);
pinkNoise = dsp.ColoredNoise(1,1e4,1);
brownNoise = dsp.ColoredNoise(2,1e4,1);
rng default;
white=whiteNoise();
pink = pinkNoise();
brown=brownNoise();

For the two parameters of MFDFA method, values of q are chosen from -5 to 5 with 101 equally spaced values and values of s are chosen from 8 to 1024 with 19 equally spaced values. Then, relative qth-order Hurst exponent curves, qth-order scaling exponent curves and multifractal spectra are drawn in Fig. 9. It is obvious that the two $h(q)$ curves are almost horizontal and, respectively, close to their theoretical values 1 and 1.5. Meanwhile, two $\tau(q)$ curves are linear with q and their slopes are respective close to 1 and 1.5. Thus, it is evidenced that the two kinds of colored noise signals are monofractal. In addition, as there are some biases between the practical value and the theoretical value, each Hurst exponent $h(q)$ curve is not horizontal strictly and each multifractal spectrum is not one point but has small width in Fig. 9. Furthermore, except for the two colored noise signals, there are other kinds of colored noise signals which are not analyzed in this paper. However, they are all monofractal [60]. Then, if the noise signals from rotary kiln are multifractal, they are not any kinds of monofractal colored noise.

Fig. 9 Characteristics of the two kinds of monofractal colored noise. (Color figure online)
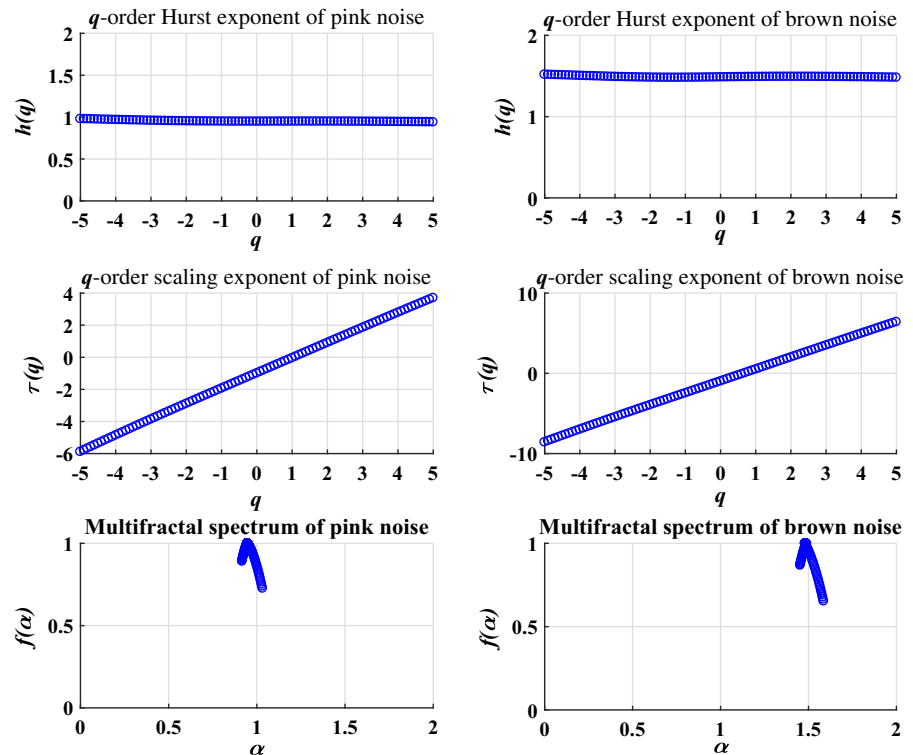
5.3 Multifractal analysis of noise from rotary kiln

Considering suggestions in papers [56,59,61,62] and several experimental results of the noise signals, values of q are chosen from -20 to 20 with 101 equally spaced values and values of s are chosen from 4 to 128 with 19 equally spaced values in this paper. Then, the qth-order scaling exponent curves, qth-order Hurst exponent curves and multifractal spectra of the noise signals from rotary kiln are, respectively, drawn in Figs. 10, 11 and 12. And it is obvious that different noises have different shapes. However, compared with relative curves in Fig. 9, the noise signals from rotary kiln also have some same characteristics which are multifractal evidents:

(1) All qth-order scaling exponent curves $\tau(q)$ are nonlinear as shown in Fig. 10.
(2) Between $q = -20$ and $q = 20$, all qth-order Hurst exponent curves are not independent of the q but decrease with the increasing of the q as shown in Fig. 11.
(3) All multifractal spectra have big width as shown in Fig. 12.

Moreover, multifractal characteristics of the noise signals are measured qualitatively as shown in Table 5, where $\Delta h = h_{\max} - h_{\min}$ is the variational range of $h(q)$. The $\Delta \alpha = \alpha_{\max} - \alpha_{\min}$ is the width of multifractal spectrum and measures the degree of fluctuation of time series, that is, the bigger the $\Delta \alpha$ is, the more drastic the fluctuation of time series is and the stronger the multifractal strength is. Generally, the bigger the values of Δh and $\Delta \alpha$ are, the stronger the multifractal strength is. Thus, based on above results, it is evidenced that the noise signals from rotary kiln are multifractal rather than the monofractal colored noise.

As is well known, the monofractal series can be characterized by the Hurst exponent (H). Namely, if $H > 0.5$, the time series is persistent and has long-range correlation. If $H < 0.5$, the time series is anti-persistent and has short-range correlation. If $H = 0.5$, the time series is uncorrelated [56,60]. For the multifractal time series, it is analyzed by using different values of q to highlight the different scale fluctuation magnitudes of time series. Namely, the positive q relates to the segments with large fluctuation magnitudes and the negative q relates to the segments with small fluctuation magnitudes. Then, in Fig. 11a, c, the Hurst expo-

Fig. 10 qth-order scaling exponent. **a** G1_wpd, **b** G1_Gao, **c** G2_wpd, **d** G2_Gao

(a)

(b)

(c)

(d)
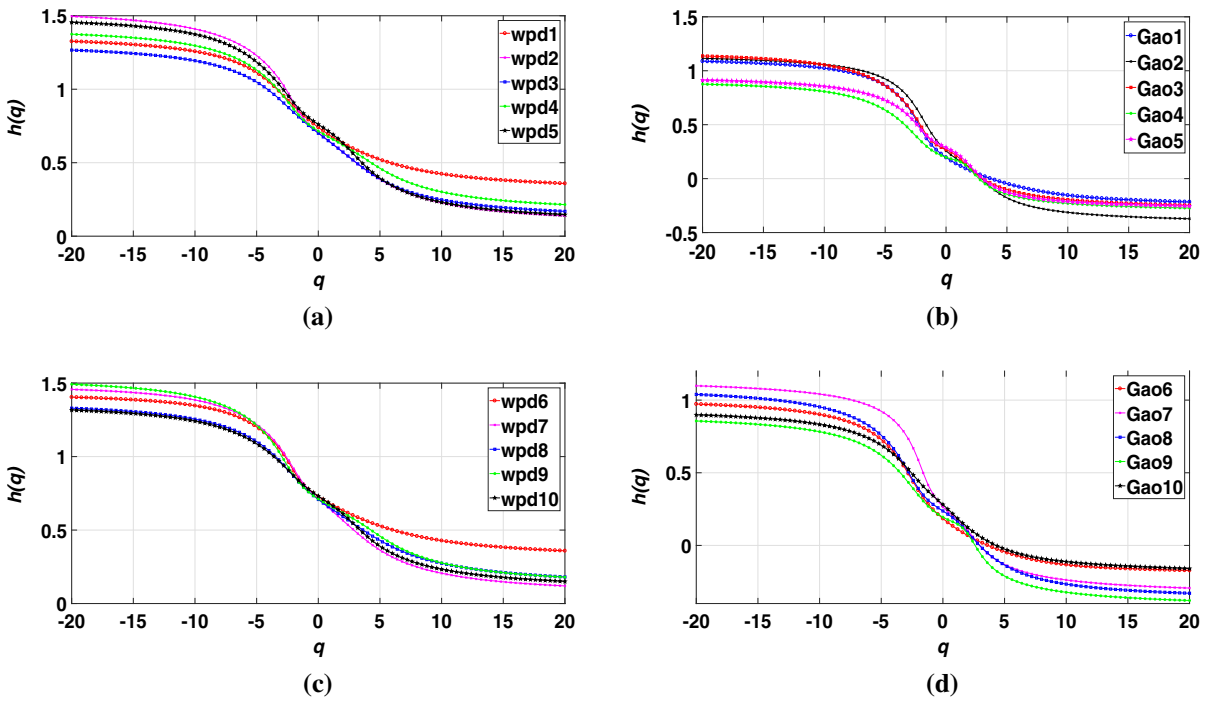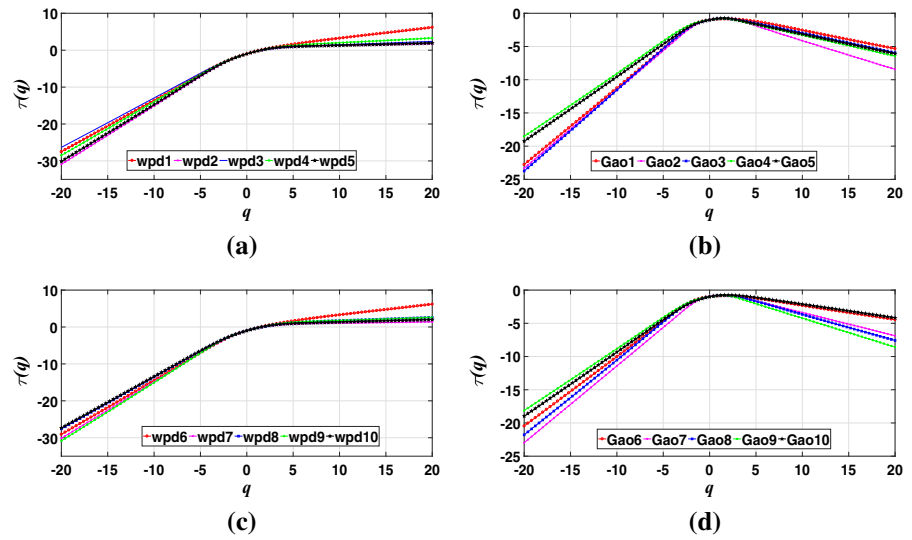
Fig. 11 qth-order Hurst exponent. **a** G1_wpd, **b** G1_Gao, **c** G2_wpd, **d** G2_Gao

(a)

(b)

(c)

(d)

nents of all the small fluctuation magnitudes and a little large fluctuation magnitudes of noise signals are bigger than 0.5, that is, they are persistent long-range correlative. For Fig. 11b, d, the Hurst exponents of all the large fluctuation magnitudes and a little small fluctuation magnitudes of noise signals are smaller than 0.5, that is, they are anti-persistent short-range correlative.

Thus, the noise signals from rotary kiln have both the persistent long-range correlation and the anti-persistent short-range correlation. Moreover, the two contradictory features interact and together decide the whole correlation and fluctuation of each noise from rotary kiln, which means the intrinsic dynamic mechanisms
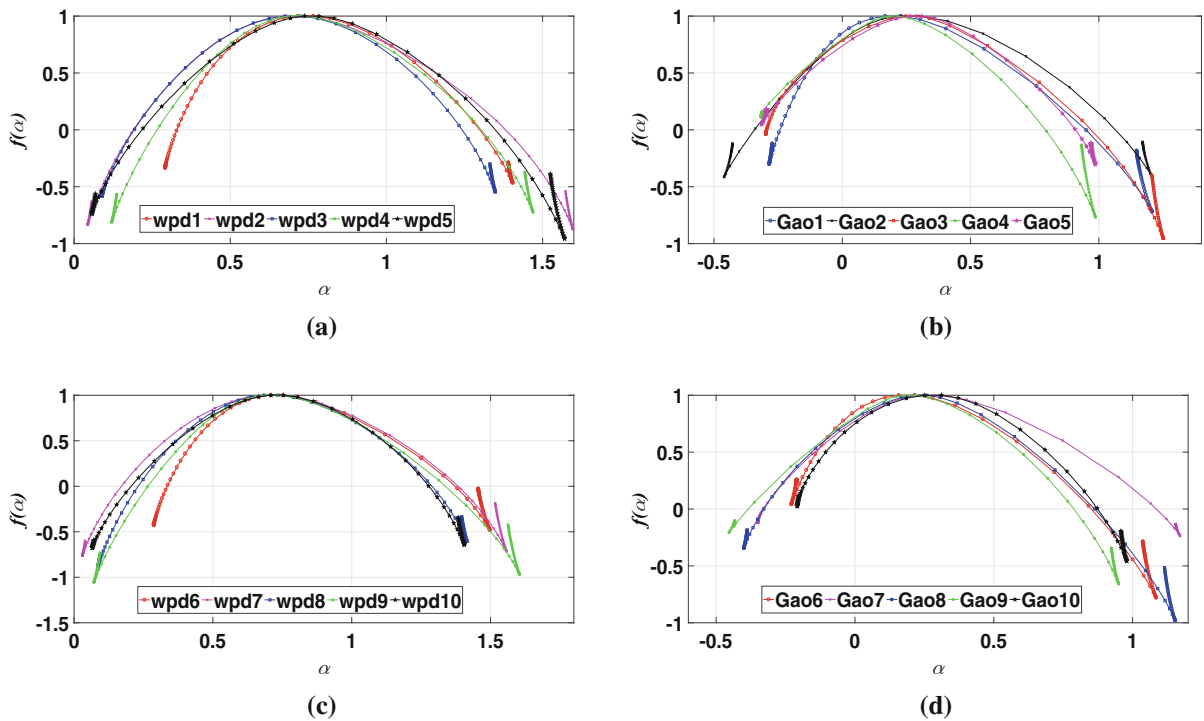
Fig. 12 Multifractal spectra. **a** G1_wpd, **b** G1_Gao, **c** G2_wpd, **d** G2_Gao

Table 5 Multifractal behaviors of original noise from rotary kiln (the Δh is the variational range of $h(q)$ and the $\Delta \alpha$ is the width of multifractal spectrum)

	Δh	$\Delta \alpha$		Δh	$\Delta \alpha$
wpd1	0.9674	1.1127	Gao1	1.3049	1.4924
wpd2	1.3581	1.5536	Gao2	1.4871	1.6688
wpd3	1.0973	1.2590	Gao3	1.3893	1.5497
wpd4	1.1596	1.3486	Gao4	1.1482	1.3038
wpd5	1.3087	1.5140	Gao5	1.1671	1.3014
wpd6	1.0456	1.2106	Gao6	1.1451	1.3136
wpd7	1.3373	1.5275	Gao7	1.3919	1.5206
wpd8	1.1483	1.3296	Gao8	1.3681	1.5542
wpd9	1.3120	1.5329	Gao9	1.2353	1.4034
wpd10	1.1662	1.3402	Gao10	1.0575	1.1869

of the noise from rotary kiln are more complex than those of monofractal colored noise signals.

For the time series with the anti-persistent short-range correlation, the tendency of two points at adjacent times of series is opposite and the whole series will always revert to its mean value [56,60], that is, the anti-persistent short-range correlation will increase the difficulty of effective prediction. Then, the anti-persistent short-range correlation is a reason why the determinate noise from rotary kiln cannot be predicted

by some models. But those unsuccessful predictions of the noise from rotary kiln do not indicate that the noise from rotary kiln is unpredictable.

5.4 Multifractal source of noise from rotary kiln

The two contradictory multifractal characteristics make the dynamic behaviors of the noise signal from rotary kiln become more complex. Then, the source of multi-

Table 6 Multifractal behaviors of shuffled noise from rotary kiln (the Δh is the variational range of $h(q)$ and the $\Delta\alpha$ is the width of multifractal spectrum)

	Δh	$\Delta\alpha$		Δh	$\Delta\alpha$
wpd1	0.1534	0.3066	Gao1	0.5292	0.8658
wpd2	0.0480	0.1015	Gao2	0.0736	0.1643
wpd3	0.0766	0.1615	Gao3	0.2076	0.4565
wpd4	0.0933	0.1918	Gao4	0.3777	0.6341
wpd5	0.0645	0.1495	Gao5	0.3484	0.5735
wpd6	0.0701	0.1497	Gao6	0.0937	0.1939
wpd7	0.1252	0.2506	Gao7	0.3034	0.5624
wpd8	0.0890	0.1957	Gao8	0.3675	0.6778
wpd9	0.0763	0.2038	Gao9	0.2705	0.5323
wpd10	0.1149	0.2509	Gao10	0.1374	0.2668

fractality of the noise from rotary kiln should be further explored and analyzed. In general, there are two main kinds of multifractality that could be distinguished [56,63]. One is generated by the diverse long-range temporal correlations of small and large fluctuations. However, this kind of temporal correlation could be removed by the shuffling procedure. Then, relative qth-order Hurst exponent $h(q)$ becomes a constant 0.5, that is, the shuffled series is no longer multifractal. The other is owing to the wide probability density distribution of the time series, and this kind of multifractality could not be destroyed by the shuffling procedure, that is, the relative qth-order Hurst exponent $h(q)$ has no change after shuffling. Furthermore, if the shuffled series still shows multifractal but becomes weaker, it means the two factors are both present. Besides, the shuffling procedure is introduced in [63,64].

In order to ensure each noise series from rotary kiln is shuffled enough, all values in each noise series are randomly interchanged for 200,000 times [56,63]. Then, the Δh and $\Delta\alpha$ of shuffled noise signals from rotary kiln are calculated by the MFDFA method and the results are listed in Table 6. Compared with the relative values in Table 5, it is obvious that the multifractality could not be destroyed fully, but all the values become much smaller. Even many values in Table 6 leave one tenth of relative values in Table 5. Thus, the two factors are both present for the multifractality of noise signals from rotary kiln. In particular, the long-range temporal correlation is the main factor for generating the multifractality of the noise from rotary kiln. Further, it also implies that the persistent long-range correlation is the main characteristic compared with

the anti-persistent short-range correlation, that is, the anti-persistent short-range correlation only increases the difficulty of prediction but cannot negate the noise from rotary kiln are predictable.

6 Conclusion

In this paper, the chaotic and multifractal characteristics of the noise of thermal variables from the rotary kiln are analyzed to explore some intrinsic dynamic characteristics of the noise. The analyzed results of the noise signals are not the same. However, based on experimental results, still five common characteristics are discovered firstly.

(1) Those noise signals are neither the white noise nor monofractal colored noise signals.
(2) Those noise signals all have the high-dimensional chaotic characteristic, which implies the noise signals are deterministic and theoretically predictable for short term.
(3) Those noise signals all have both persistent and anti-persistent multifractal characteristics, which means dynamic mechanisms of those noise signals from rotary kiln are more complex than that of monofractal colored noise signals.
(4) The anti-persistent multifractal characteristic is a reason why determinate noise signals from rotary kiln cannot be successfully predicted, but it cannot negate the predictable of noise from rotary kiln.
(5) The multifractality of those noise signals are generated by the long-term temporal correlation and

wide probability density distribution together. In particular, the former is the main factor.

Further, based on the discoveries in the paper, previous works of multifractal theories and models, two ideas about modeling multifractality of the noise signals are proposed below as the warm-up for modeling the noise from rotary kiln in future.

(1) Data-based model. The fractal is used to measure the self-similarity relationship between the part and the whole. Moreover, the multifractal process could be regarded as the amalgamation of the infinite number of monofractal subprocesses and each monofractal subprocess is characterized by a single Holder exponent. Then, it may be a feasible idea that the multifractality of noise signals from rotary kiln may be constructed by some monofractal signals with some characteristics. Moreover, the key of construction is to recurrence the complex relationship of the interaction of subprocesses as accurately as possible. And many neural network models may be candidates. Furthermore, it also need to consider the kind of monofractal series.

(2) Mathematic model. Some economists proposed many multifractal models to model financial time series. The volatilities of many financial data are random-like but hierarchical in nature, which is similar to the noise signals from rotary kiln. Then, those multifractal models are inspirations for modeling the noise. However, as those multifractal models are based on some assumptions which may be not fit for the noise signals, they should not be used directly but be improved.

The presence of chaotic and multifractal characteristics in the noise from rotary kiln will change the view about noise and expand new methods to deal with the noise. In particular, it will improve some filtering algorithms of industrial signals, mechanism-based modeling methods and control strategies based on the hypothesis of the white noise and the monofractal colored noise. Furthermore, it will also offer some enlightenment for other fields.

Compliance with ethical standards

Conflict of interest The authors declare that they have no conflict of interest.

A Appendix

A.1 The wavelet packet decomposition method

The steps of noise extraction based the wavelet packet decomposition (WPD) method are introduced as follows. Moreover, please see Ref. [46,47] for the more details.

Step 1. The wavelet packet decomposition (WPD) and the confirmation of the best basis. In the point of view of compression, the standard wavelet transform may not produce the best result, since it is limited to wavelet bases that increase by a power of two toward the low frequencies, that is, the best basis of the WPD should be found out after the WPD. Moreover, the best basis corresponds to the minimum entropy or maximum information for the distribution of coefficients [46]. In this paper, the first step can be realized using the command "wpdec" in MATLAB.

Step 2. The confirmation of the thresholding value. Generally, small coefficients are mostly noises and large coefficients contain the actual signal. Then, a thresholding value should be proposed to distinguish small coefficients and large coefficients. The penalization method is proposed to calculate the universal thresholding value and can be realized using the command "wpbmpen" in MATLAB.

Step 3. The reconstruction of the signal based on wavelet transform. Donoho [47] pointed out that only coefficients whose absolute value is higher than the predefined threshold value is retained. Then, in this paper, the soft thresholding method [47] is used to replace wavelet transform coefficients as follows:

$$l = 2: \quad Signal: \quad \underbrace{s_1 \quad s_2}_{\bar{s}_1} \cdots \underbrace{s_3 \quad s_4}_{\bar{s}_2} \cdots \underbrace{s_5 \quad s_6}_{\bar{s}_3} \cdots \underbrace{s_i \quad s_{i+1}}_{\bar{s}_i = (s_i + s_{i+1})/2} \cdots$$

$$l = 2: \quad Noise: \quad x_1 \quad x_2 \cdots x_3 \quad x_4 \cdots x_5 \quad x_6 \cdots x_i \quad x_{i+1} = s_{i+1} - \bar{s}_i$$

$$\cdots$$

$$l = k: \quad Signal: \quad \underbrace{s_1 \quad s_1 \quad \cdots \quad s_k}_{\bar{s}_1} \cdots \underbrace{s_i \quad s_{i+1} \quad \cdots \quad s_{i+k-1}}_{\bar{s}_j = (s_i + s_{i+1} + \cdots + s_{i+k-1})/k} \cdots$$

$$l = k: \quad Noise: \quad x_1 \quad x_2 \quad \cdots \quad x_k \cdots x_i \quad x_{i+1} \quad \cdots \quad x_{i+k-1} = s_{i+k-1} - \bar{s}_j$$

Fig. 13 Illustration of noise extraction using the Gao method. The s_i is the value of the thermal signal of rotary kiln, $\bar{s}_i$ and $\bar{s}_j$ are the mean value, and x_i is the value of the extracted noise signal

$$Rw_i^p = \begin{cases} 0, & \text{if } |w_i^p| < \text{thr} \\ \text{sign}(w_i^p)(|w_i^p| - thr), & \text{if } |w_i^p| > \text{thr} \end{cases} \tag{22}$$

where the w_i^p is the wavelet transform coefficient of the ith sub-signal in the pth level, the Rw_i^p is the replace wavelet transform coefficient of the ith sub-signal in the pth level and the thr is the universal threshold which is calculated by the penalization method [47]. After replacing wavelet transform coefficients, the retained coefficients are used to reconstruct the useful signal. And the denoise procedure is realized using the command "wpdencmp" in Matlab.

Step 4. The noise signal is extracted through subtracting the useful signal from the original signal.

A.2 The Gao method

The Gao method [65] is a moving average method in nature, and the illustration of noise extraction using the Gao method is shown in Fig. 13. Moreover, the procedure is introduced as follows.

Step 1. From the head to the end, l signal points are selected as a segment in turn.

Step 2. The average value of each segment is calculated.

Step 3. The average value of each segment is subtracted by the l signal values of relative segment. Then, l noise values in each segment are extracted.

Step 4. The whole noise time series are extracted.

The higher frequency of noise, the smaller the value of the l is selected [65]. In our paper, we set $l = 2$, that

is, two points of signals are selected as a segment in turn and the average value $\bar{s}_i = (s_i + s_{i+1})/2$ is calculated. Then, each value of noise is calculated through $x_{i+1} = s_{i+1} - \bar{s}_i$.

References

1. Xu, Y., Jia, Y., Wang, H., Liu, Y., Wang, P., Zhao, Y.: Spiking activities in chain neural network driven by channel noise with field coupling. Nonlinear Dyn. **95**(4), 3237–3247 (2019). https://doi.org/10.1007/s11071-018-04752-2
2. Davies, H.G.: Slow sinusoidal modulation through bifurcations: the effect of additive noise. Nonlinear Dyn. **36**(2), 217–228 (2004)
3. Montillet, J., Tregoning, P., McClusky, S., Yu, K.: Extracting white noise statistics in gps coordinate time series. IEEE Geosci. Remote Sens. Lett. **10**(3), 563–567 (2013)
4. Yang, Y., Wei, X., Jia, W., Han, Q.: Stationary response of nonlinear system with caputo-type fractional derivative damping under Gaussian white noise excitation. Nonlinear Dyn. **79**(1), 139–146 (2015)
5. Qi, L., Cai, G.Q.: Dynamics of nonlinear ecosystems under colored noise disturbances. Nonlinear Dyn. **73**(1), 463–474 (2013)
6. Lei, Y., Hua, M., Lin, D.: Onset of colored-noise-induced chaos in the generalized duffing system. Nonlinear Dyn. **89**(2), 1371–1383 (2017)
7. Fokou, I.S.M., Buckjohn, C.N.D., Siewe, M.S., Tchawoua, C.: Probabilistic distribution and stochastic p-bifurcation of a hybrid energy harvester under colored noise. Commun. Nonlinear Sci. Numer. Simul. **56**, 177–197 (2018)
8. Yang, C., Gao, Z., Liu, F.: Kalman filters for linear continuous-time fractional-order systems involving coloured noises using fractional-order average derivative. IET Control Theory Appl. **12**(4), 456–465 (2018)
9. Tang, T., Jia, L., Lou, J., Tao, R., Wang, Y.: Adaptive eiv-fir filtering against coloured output noise by using linear prediction technique. IET Signal Proc. **12**(1), 104–112 (2018)
10. Vasseur, D., Yodzis, P.: The color of environmental noise. Ecology **85**, 1146–1152 (2004)
11. Grinsted, A., Moore, J.C., Jevrejeva, S.: Application of the cross wavelet transform and wavelet coherence to geophysical time series. Nonlinear Process. Geophys. **11**(5/6), 561–566 (2004)
12. Schulz, M., Mudelsee, M.: Redfit: estimating red-noise spectra directly from unevenly spaced paleoclimatic time series. Comput. Geosci. **28**(3), 421–426 (2002)
13. Koscielny-Bunde, E., Bunde, A., Havlin, S., Roman, H.E., Goldreich, Y., Schellnhuber, H.-J.: Indication of a universal persistence law governing atmospheric variability. Phys. Rev. Lett. **81**, 729–732 (1998)
14. Kasdin, N.J.: Discrete simulation of colored noise and stochastic processes and 1/f/sup /spl alpha// power law noise generation. Proc. IEEE **83**(5), 802–827 (1995)
15. Viswanathan, R.: On the autocorrelation of complex envelope of white noise. IEEE Trans. Inf. Theory **52**(9), 4298–4299 (2006)

16. Ostry, D.I.: Synthesis of accurate fractional Gaussian noise by filtering. IEEE Trans. Inf. Theory **52**(4), 1609–1623 (2006)

17. Kaulakys, B.: On the intrinsic origin of 1/f noise. Microelectron. Reliab. **40**(11), 1787–1790 (2000)

18. Hung, Y.-C., Struzik, Z.R., Chin-Kun, H.: Noise as a potential controller in antagonist inter-reacting systems. Physica A **512**, 500–506 (2018)

19. Poxon, J., Jennings, P., Allman-Ward, M.: Development of a hybrid electric vehicle (HEV) model for interactive customer assessment of sound quality. In: IET HEVC 2008—Hybrid and Eco-Friendly Vehicle Conference, pp. 1–4 (2008)

20. Garmendia, N., Portilla, J.: Investigations of AM, PM noise, and noise figure in an SiGe-HBT amplifier operating in linear and nonlinear regimes. IEEE Trans. Microw. Theory Tech. **58**(4), 807–813 (2010)

21. Revoredo, T., Mora-Camino, F., Slama, J.: A two-step approach for the prediction of dynamic aircraft noise impact. Aerosp. Sci. Technol. **59**, 122–131 (2016)

22. Filippone, A.: Aircraft noise prediction. Prog. Aerosp. Sci. **68**, 27–63 (2014)

23. Hao, W., Li, K., Shi, W., Clarke, K.C., Zhang, J., Li, H.: A wavelet-based hybrid approach to remove the flicker noise and the white noise from GPS coordinate time series. GPS Solut. **19**(4), 511–523 (2015)

24. Muhammad, N., Bibi, N., Jahangir, A., Mahmood, Z.: Image denoising with norm weighted fusion estimators. Pattern Anal. Appl. **21**(4), 1013–1022 (2018)

25. Muhammad, N., Bibi, N., Wahab, A., Mahmood, Z., Akram, T., Naqvi, S.R., Oh, H.S., Kim, D.-G.: Image de-noising with subband replacement and fusion process using Bayes estimators. Comput. Electr. Eng. **70**, 413–427 (2018)

26. Mughal, B., Muhammad, N., Sharif, M., Rehman, A., Saba, T.: Removal of pectoral muscle based on topographic map and shape-shifting silhouette. BMC Cancer **18**(1), 778 (2018)

27. Khalid, S., Muhammad, N., Sharif, M.: Automatic measurement of the traffic sign with digital segmentation and recognition. IET Intell. Transp. Syst. **13**, 269–279 (2019)

28. Casalino, D., Diozzi, F., Sannino, R., Paonessa, A.: Aircraft noise reduction technologies: a bibliographic review. Aerosp. Sci. Technol. **12**(1), 1–17 (2008). (Aircraft noise reduction)

29. Crupi, F., Giusi, G., Ciofi, C., Pace, C.: Enhanced sensitivity cross-correlation method for voltage noise measurements. IEEE Trans. Instrum. Meas. **55**(4), 1143–1147 (2006)

30. Thompson, J.R., Wilson, J.R.: Multifractal detrended fluctuation analysis: practical applications to financial time series. Math. Comput. Simul. **126**, 63–88 (2016)

31. Gao, C., Qian, J.: Evidence of chaotic behavior in noise from industrial process. IEEE Trans. Signal Process. **55**(6), 2877–2884 (2007)

32. Packard, N.H., Crutchfield, J.P., Farmer, J.D., Shaw, R.S.: Geometry from a time series. Phys. Rev. Lett. **45**, 712–716 (1980)

33. Takens, F.: Detecting strange attractors in turbulence. In: Rand, D., Young, L.-S. (eds.) Dynamical Systems and Turbulence, Warwick 1980, pp. 366–381. Springer, Berlin (1981)

34. Theiler, J., Eubank, S., Longtin, A., Galdrikian, B., Farmer, J.D.: Testing for nonlinearity in time series: the method of surrogate data. Physica D Nonlinear Phenom. **58**(1), 77–94 (1992)

35. Theiler, J., Eubank, S.: Don't bleach chaotic data. Chaos **3**(4), 771–782 (1993)

36. Small, M., Dejin, Y., Harrison, R.G.: Surrogate test for pseudoperiodic time series data. Phys. Rev. Lett. **87**, 188101 (2001)

37. Schreiber, T., Schmitz, A.: Surrogate time series. Physica D **142**(3), 346–382 (2000)

38. Thiel, M., Romano, M.C., Kurths, J., Rolfs, M., Kliegl, R.: Twin surrogates to test for complex synchronisation. Europhys. Lett. (EPL) **75**(4), 535–541 (2006)

39. Lancaster, G., Iatsenko, D., Pidde, A., Ticcinelli, V., Stefanovska, A.: Surrogate data for hypothesis testing of physical systems. Phys. Rep. **748**, 1–60 (2018)

40. Theiler, J.: On the evidence for low-dimensional chaos in an epileptic electroencephalogram. Phys. Lett. A **196**(5), 335–341 (1995)

41. Schreiber, T., Schmitz, A.: Improved surrogate data for nonlinearity tests. Phys. Rev. Lett. **77**, 635–638 (1996)

42. Calvet, L.E., Fisher, A.J.: How to forecast long-run volatility: regime switching and the estimation of multifractal processes. J. Financ. Econom. **2**(1), 49–83 (2004)

43. Mandelbrot, B., Fisher, A., Calvet, L.: A multifractal model of asset returns. Cowles Foundation Discussion Papers 1164, Cowles Foundation for Research in Economics, Yale University (1997)

44. Lux, T.: The Markov-switching multifractal model of asset returns. J. Bus. Econ. Stat. **26**(2), 194–210 (2008)

45. Schreiber, T.: Extremely simple nonlinear noise-reduction method. Phys. Rev. E **47**, 2401–2404 (1993)

46. Walczak, B., Massart, D.L.: Noise suppression and signal compression using the wavelet packet transform. Chemometr. Intell. Lab. Syst. **36**(2), 81–94 (1997)

47. Donoho, D.L.: De-noising by soft-thresholding. IEEE Trans. Inf. Theory **41**(3), 613–627 (1995)

48. Xia, C., Song, P., Shi, T., Yan, Y.: Chaotic dynamics characteristic analysis for matrix converter. IEEE Trans. Industr. Electron. **60**(1), 78–87 (2013)

49. Rao, X.-B., Chu, Y.-D., Lu-Xu, Chang, Y.-X., Zhang, J.-G.: Fractal structures in centrifugal flywheel governor system. Commun. Nonlinear Sci. Numer. Simul. **50**, 330–339 (2017)

50. Kennel, M.B., Brown, R., Abarbanel, H.D.I.: Determining embedding dimension for phase-space reconstruction using a geometrical construction. Phys. Rev. A **45**, 3403–3411 (1992)

51. Fraser, A.M., Swinney, H.L.: Independent coordinates for strange attractors from mutual information. Phys. Rev. A **33**, 1134–1140 (1986)

52. Wolf, A., Swift, J.B., Swinney, H.L., Vastano, J.A.: Determining Lyapunov exponents from a time series. Physica D **16**(3), 285–317 (1985)

53. Bolotin, Y., Tur, A., Yanovsky, V.: Chaos: Concepts, Control and Constructive Use. Springer, Berlin (2017)

54. Nakamura, T., Small, M.: Applying the method of small-shuffle surrogate data: testing for dynamics in fluctuating data with trends. Int. J. Bifurc. Chaos **16**(12), 3581–3603 (2006)

55. Parlitz, U., Kocarev, L.: Using surrogate data analysis for unmasking chaotic communication systems. Int. J. Bifurc. Chaos **07**(02), 407–413 (1997)

56. Kantelhardt, J.W., Zschiegner, S.A., Koscielny-Bunde, E., Havlin, S., Bunde, A., Stanley, H.E.: Multifractal detrended fluctuation analysis of nonstationary time series. Physica A Stat. Mech. Appl. **316**(1), 87–114 (2002)

57. Feder, J.: Fractals. Springer, Boston, MA (1988)

58. Peitgen, H.O., Jürgens, H., Saupe, D.: Chaos and Fractals. Springer, New York, NY (2004)

59. Ihlen, E.A.F.: Introduction to multifractal detrended fluctuation analysis in Matlab. Front. Physiol. **3**, 141 (2012)

60. Beran, S.G.R.K.J., Feng, Y.: Long-Memory Processes: Probabilistic Properties and Statistical Methods. Springer, Berlin (2013)

61. Tang, J., Wang, D., Fan, L., Zhuo, R., Zhang, X.: Feature parameters extraction of GIS partial discharge signal with multifractal detrended fluctuation analysis. IEEE Trans. Dielectr. Electr. Insul. **22**(5), 3037–3045 (2015)

62. Livi, L., Sadeghian, A., Sadeghian, H.: Discrimination and characterization of Parkinsonian rest tremors by analyzing long-term correlations and multifractal signatures. IEEE Trans. Biomed. Eng. **63**(11), 2243–2249 (2016)

63. Cao, G., He, L.Y., Cao, J.: Multifractal Detrended Analysis Method and Its Application in Financial Markets. Springer, Singapore (2018)

64. Matia, K., Ashkenazy, Y., Stanley, H.E.: Multifractal properties of price fluctuations of stocks and commodities. EPL (Europhys. Lett.) **61**(3), 422 (2003)

65. Gao, C., Qian, J.: Evidence of chaotic behavior in noise from industrial process. IEEE Trans. Signal Process. **55**(6), 2877–2884 (2007)